

# Contribution of TADF and Exciplex Emission for Efficient “Warm-White” OLEDs

Gintare Grybauskaite-Kaminskiene,<sup>a</sup> Khrystyna Ivaniuk,<sup>b</sup> Gintautas Bagdziunas,<sup>a</sup> Pavlo Turyk,<sup>b</sup> Pavlo Stakhira,<sup>b</sup> Gleb Baryshnikov,<sup>c,d</sup> Dmytro Volyniuk,<sup>a</sup> Vladyslav Cherpak,<sup>c</sup> Boris Minaev,<sup>c,d</sup> Zenon Hotra,<sup>b,f</sup> Hans Ågren,<sup>c</sup> Juozas Vidas Grazulevicius<sup>a</sup>

## Abstract

Bicarbazole derivative 4,4'-(9H,9'H-[3,3'-bicarbazole]-9,9'-diyl)bis(3-(trifluoromethyl)benzotrile), denoted as *p*CNBCzoCF<sub>3</sub> was synthesized and tested for white OLED applications. *p*CNBCzoCF<sub>3</sub> demonstrated extremely small value of the singlet-triplet energy gap that caused intensive thermally-activated delayed fluorescence (TADF). In addition, this compound is able to form exciplex-type excited states at the interface with star-shaped 4,4',4''-tris[phenyl(*m*-tolyl)amino]triphenylamine (*m*-MTDATA). Combining TADF emission of *p*CNBCzoCF<sub>3</sub> with the exciplex emission from the *p*CNBCzoCF<sub>3</sub>/*m*-MTDATA interface we fabricated a number of highly efficient “warm-white” OLEDs electroluminescence of which were close to candle emission. The best device demonstrated very high brightness of 40900 Cd/m<sup>2</sup> (at 15 V), current efficiency of 53.8 Cd/A and power efficiency of 19.3 lm/W, while the external quantum efficiency reached 18.8 %. The fabricated devices demonstrated high emission characteristics even for the standard test at 1000 Cd/m<sup>2</sup> (current efficiency of 46.2 Cd/A, power efficiency of 10.6 lm/W, EQE of 17.0 %).

## Introduction

Fabrication of highly luminous warm-white light-emitting multilayered devices on thin flat substrates opens up promising lighting sources for residential space and display applications.<sup>1-5</sup> During recent years a considerable and sustainable improvement has been witnessed for lighting characteristics of organic light-emitting devices (OLEDs), primarily reflecting the progress in design and synthesis of organic materials exhibiting thermally-activated delayed fluorescence (TADF).<sup>6-12</sup> TADF is usually observed for molecules that are characterized by quasi-degenerate first singlet (S<sub>1</sub>) and first triplet (T<sub>1</sub>) excited states, i.e. with singlet-triplet gaps ( $\Delta E_{ST}$ ) being at the *kT* scale, making it possible to activate the spin-forbidden T<sub>1</sub>→S<sub>1</sub> transition by thermal influence. TADF-based OLEDs usually demonstrate high internal quantum efficiency (IQE) by converting nearly 100% of the injected carriers into photons. The design and synthesis of highly efficient TADF materials is, however, rather difficult task because of the very sensitive balance between T<sub>1</sub>→S<sub>1</sub> reverse inter-system crossing (RISC) and the radiative decay by S<sub>1</sub>→S<sub>0</sub> transition. As a general trend, the RISC probability increases with the constriction of the  $\Delta E_{ST}$  gap.<sup>13</sup> A good way to achieve small  $\Delta E_{ST}$  gap values is to manipulate the space separation of HOMO and LUMO wave-functions by breaking up  $\pi$ -conjugation between donor (D) and acceptor (A) moieties in organic molecular materials, for example by a mutual rotation of D and A fragments along a  $\sigma$ -bond.<sup>13</sup> However, an orthogonal orientation between D and A fragments inhibits the radiative decay upon S<sub>1</sub>→S<sub>0</sub> transition that causes low TADF intensity. A compromise solution for this problem could be the partial mutual rotation of D and A moieties stabilized by the intramolecular interactions that provides non-zero electron

<sup>a</sup>Department of Polymer Chemistry and Technology, Kaunas University of Technology, Radvilenu Plentas 19, LT-50254, Kaunas, Lithuania.

<sup>b</sup>Lviv Polytechnic National University, S. Bandera 12, 79013 Lviv, Ukraine.

<sup>c</sup>Division of Theoretical Chemistry and Biology, School of Biotechnology, KTH Royal Institute of Technology, 10691 Stockholm, Sweden.

<sup>d</sup>Bohdan Khmelnytsky National University, Shevchenko 81, 18031 Cherkassy, Ukraine.

<sup>e</sup>School of Materials Science and Engineering, Georgia Institute of Technology, Atlanta, Georgia 30332, United States.

<sup>f</sup>Rzeszów University of Technology, W. Pola 2, Rzeszów 35-959, Poland.

density in the common molecular fragments.<sup>14,15</sup> Such HOMO-LUMO configurations make it possible to characterize the  $S_1 \rightarrow S_0$  transition by an intensity that is sufficiently high for utilization in TADF-based OLEDs. Although the number of TADF materials grows significantly every year, it still remains limited comparing with “wide-gap” fluorophores and phosphors.

Recently, a new family of bicarbazole-based TADF materials was synthesized through a simple one-step catalyst-free C–N coupling reaction, by using 9H,9'H-3,3'-bicarbazole and alkyl substituted fluorocyanobenzene as starting reagents.<sup>16</sup> These compounds were used as host materials for another type of TADF green dopant 2,3,5,6-tetra(9H-carbazol-9-yl)-4-cyano-pyridine (**4CzCNPy**). All the devices described in ref.<sup>16</sup> exhibit only green electroluminescence (EL) of **4CzCNPy**, while no emission from the host bicarbazole-based materials was observed. In the present work we take this idea a step further by using the material not only as host matrix but also involving it in the emission process. We thereby take into account the fact that carbazole derivatives are able to form exciplexes at organic-organic interfaces with star-shaped molecules,<sup>5</sup> a feature which, as we show here, can be used for broadening of EL spectra of OLEDs.

In the present work we studied behaviour in OLED of bicarbazole-based TADF material 4,4'-(9H,9'H-[3,3'-bicarbazole]-9,9'-diyl)bis(3-(trifluoromethyl)benzotrile) (Scheme S1), named as **pCNBCzoCF<sub>3</sub>**, the synthesis of which was reported recently<sup>16</sup>. In contrast to the previous work, we here propose to use **pCNBCzoCF<sub>3</sub>** as both the emissive and exciplex-forming material for the fabrication of white OLED (WOLED). Combining TADF emission of **pCNBCzoCF<sub>3</sub>** with the exciplex emission from the organic-organic interface between **pCNBCzoCF<sub>3</sub>** and the layers of star-shaped 4''-tris[phenyl(*m*-tolyl)amino]triphenylamine (***m*-MTDATA**) we fabricated highly-efficient WOLEDs with a warm-white emission.

### Computational details

A theoretical interpretation of the electronic spectra of **pCNBCzoCF<sub>3</sub>** was performed by the time dependent (TD)<sup>17</sup> density functional theory (DFT) method using the common three-parameterized exchange-correlation B3LYP functional<sup>18,19</sup> with the 6-31G(d)<sup>20</sup> basis set in the vacuum approximation and also within the polarizable continuum model (PCM)<sup>21</sup> for accounting the effect of an embedding tetrahydrofuran (THF). In both cases we have used the equilibrium geometries of **pCNBCzoCF<sub>3</sub>** optimized in vacuum approximation and in THF, respectively, by the same B3LYP/6-31G(d) method. All the calculations were carried out using the Gaussian 09 program package.

### Experimental methods

The synthesis of 4,4'-(9H,9'H-[3,3'-bicarbazole]-9,9'-diyl)bis(3-(trifluoromethyl)benzotrile) (**pCNBCzoCF<sub>3</sub>**)<sup>16</sup> is described in SI.

Photoluminescence (PL) and UV spectra of thin films prepared by the vacuum deposition technique were recorded with the Edinburgh Instruments FLS980 and PerkinElmer Lambda 25 spectrometers, respectively. To separate the phosphorescence spectra of the film of **pCNBCzoCF<sub>3</sub>**, the emission spectrum was recorded at 77 K with the delay time exceeding 50 ms.<sup>22-24</sup> Edinburgh Instruments FLS980 spectrometer and PicoQuant LDH-D-C-375 laser (wavelength 374 nm) as the excitation source were used for recording PL decay curves and PL intensity dependencies on laser flux of samples at room temperature. Characterization of photophysical properties of the samples at different temperatures in inert atmosphere (N<sub>2</sub>) was performed using a variable temperature liquid nitrogen cryostat (Optistat DN2).

Three types of OLEDs were fabricated by means of vacuum deposition of organic semiconductor layers and metal electrodes onto a pre-cleaned ITO-coated glass substrate under vacuum of 10<sup>-5</sup>Torr:

A) ITO/CuI/TCTA/**pCNBCzoCF<sub>3</sub>**/BCP/Ca:Al

B) ITO/CuI/*m*-MTDATA/*p*CNBCzoCF<sub>3</sub>/BCP/Ca:Al

C) ITO/CuI/TCTA/*p*CNBCzoCF<sub>3</sub>/*m*-MTDATA/*p*CNBCzoCF<sub>3</sub>/BCP/Ca:Al

The devices were fabricated by stepwise deposition of the different organic layers. The chemical structures of organic compounds used for the fabrication of devices A-C are presented in Figure 1. CuI was used as a hole-injection layer.<sup>25</sup> Tris(4-carbazoyl-9-ylphenyl)amine (TCTA) and 4,4',4''-tris[phenyl(*m*-tolyl)amino]triphenylamine (*m*-MTDATA)<sup>26-28</sup> were used for the preparation of hole-transporting layers. *p*CNBCzoCF<sub>3</sub> was used as a fluorescent (TADF) material, while 2,9-dimethyl-4,7-diphenyl-1,10-phenanthroline (BCP)<sup>29</sup> was used for the preparation of electron-transporting layer which alleviates the stepwise electron transfer from the Ca:Al cathode to the emissive layer.

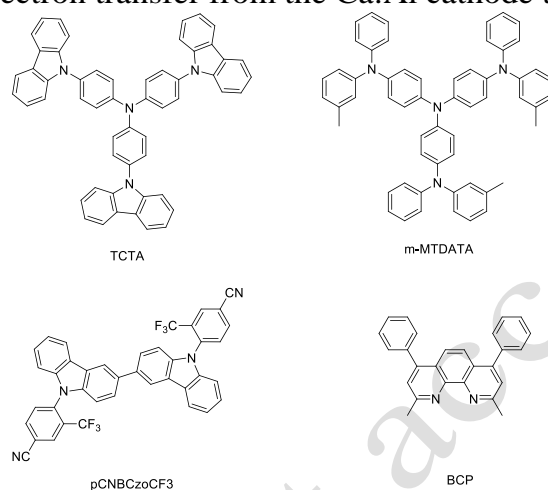


**Figure 1.** The structures of TCTA, *m*-MTDATA, *p*CNBCzoCF<sub>3</sub> and BCP.

The density–voltage and luminance–voltage dependences were recorded using a semiconductor parameter analyser HP 4145A. Measurement of brightness was obtained using a calibrated photodiode.<sup>30</sup> Electroluminescence (EL) spectra were recorded with an Ocean Optics USB2000 spectrometer. Ionization potential (IP) for the *p*CNBCzoCF<sub>3</sub> film was measured in air by the electron photoemission method as reported earlier.<sup>31</sup> The samples were fabricated by means of vacuum deposition at 10<sup>-5</sup> Torr onto fluorine doped tin oxide coated glass substrates. The experimental setup consisted of a deep-UV deuterium light source ASBN-D130-CM, a CM110 1/8m monochromator, a 6517B Keithley electrometer. Charge-transporting properties of the compound were investigated by time-of-flight (ToF) technique with setup similar to the previously described one.<sup>32</sup>

## Results and discussion

### Spectroscopic characterization of *p*CNBCzoCF<sub>3</sub>

The experimental absorption spectrum of the solution of *p*CNBCzoCF<sub>3</sub> in THF recorded at ambient conditions is presented in Figure 2 (orange line). For the comparison, the theoretical spectrum simulated by the TD DFT method accounting for the PCM model is shown in Figure 2 (blue line). The first singlet electronic transition in the spectrum of *p*CNBCzoCF<sub>3</sub> is reflected at 447.6 nm (Table 1) but appears only weakly in the experimental and theoretically simulated spectra. Accounting the fact that *p*CNBCzoCF<sub>3</sub> is a  $\sigma$ -bond coupled dimer of 4-(9H-carbazol-9-yl)-3-(trifluoromethyl)benzotrile the first singlet and triplet excited states are almost doubly degenerated. Due to the absence of strict symmetry constraints the S<sub>1</sub> and S<sub>2</sub> states are split by 0.2 nm in our calculations and the T<sub>1</sub> and T<sub>2</sub> states are split by 0.3 nm (Table 1). As it can be seen from Figure 3 both S<sub>1</sub> and S<sub>2</sub> states of *p*CNBCzoCF<sub>3</sub> are of charge transfer (CT) type and these transitions correspond

to electron density moving from 3-(trifluoromethyl)benzotrile moieties to carbazole units. It is a general rule that CT transitions are characterized by a very weak intensity and also are sensitive to the influence of a solvent.<sup>33</sup> Indeed, the energy of  $S_1$  and  $S_2$  states increase significantly in THF environment (2.77 eV) comparing with the vacuum approximation (2.64 eV).

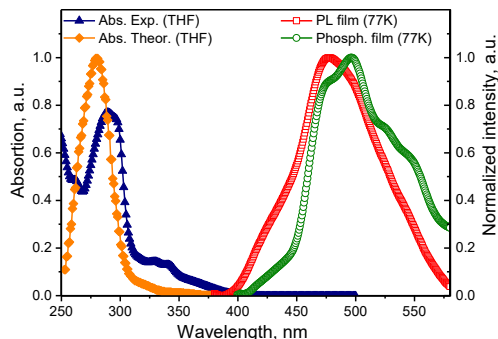


**Figure 2.** Absorption and emission spectra of *p*CN*BCzo*CF<sub>3</sub>.

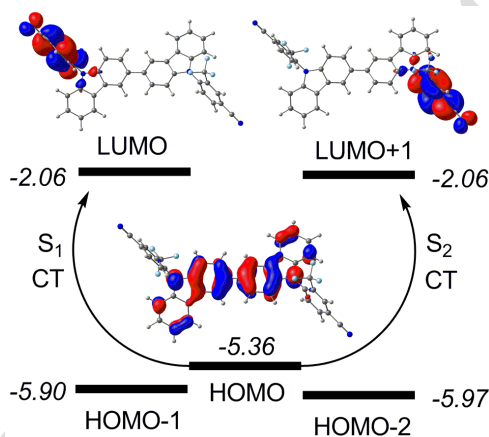


**Figure 3.** MOs levels diagram for *p*CN*BCzo*CF<sub>3</sub> (italic numbers are the MOs energies in eV).

Due to weak intensity of the  $S_0 \rightarrow S_1$  transition the photoluminescence quantum yield of *p*CN*BCzo*CF<sub>3</sub> was measured as 19.3 and 20 % for the THF solution and solid film state, respectively, indicating the dominant role of non-radiative quenching processes in the deactivation of the first excited singlet state.

The long-wavelength shoulder in the absorption spectrum of *p*CN*BCzo*CF<sub>3</sub> solution (310-370 nm) can be assigned to the manifold of weak singlet-singlet electronic transitions  $S_0 \rightarrow S_{3-14}$ . Among them the electronic transitions into  $S_5$  and  $S_{12}$  states are the most intense (Table 1). The high-intensity absorption band at ca. 290 nm corresponds to two electronic transitions  $S_0 \rightarrow S_{15}$  and  $S_0 \rightarrow S_{20}$  from the frontier occupied MOs into the high-lying unoccupied orbitals.

**Table 1.** Assignment of absorption spectrum of *p*CN*BCzo*CF<sub>3</sub> together with estimations of  $S_1$  and  $T_1$  energies.

State	$\lambda_{\text{theor.}}^{\text{abs.}}$ nm	$\lambda_{\text{exp.}}^{\text{abs.}}$ nm	$E_{\text{exp.}}/E_{\text{t}}$ heor., eV	$f$	Assignment
T <sub>1</sub>	449.4	-	2.64 <sup>a</sup> /2 .586 <sup>c</sup> /2 .757 <sup>e</sup> /2.447 <sup>f</sup>	0	HOMO → LUMO (78%)
T <sub>2</sub>	449.1	-	-	0	HOMO → LUMO+1 (78%)
S <sub>1</sub>	447.6	-	2.83 <sup>b</sup> /2 .597 <sup>d</sup> /2 .768 <sup>e</sup> /2.455 <sup>f</sup>	0.00 24	HOMO → LUMO (91%)
S <sub>2</sub>	447.4	-	-	0.00 11	HOMO → LUMO+1 (91%)
S <sub>5</sub>	349	342	-	0.02 0	HOMO → LUMO+2 (91%)
S <sub>12</sub>	318	330	-	0.06 7	HOMO → LUMO+5 (88%)
S <sub>15</sub>	289	289	-	0.52 5	HOMO → LUMO+6 (79%)
S <sub>20</sub>	281	-	-	1.10 3	HOMO-1 → LUMO+4 (67%)

a) Estimated from the phosphorescence spectrum (at 77 K) in Ref 16.

b) Estimated from fluorescence spectrum (at 77 K) in Ref 16.

c) Estimated from the phosphorescence spectrum of solid film (at 77 K) in this work.

d) Estimated from the photoluminescence spectrum of solid film (at 77 K) in this work.

e) Calculated by the TDDFT B3LYP/6-31G(d) method with PCM model (THF)

f) Calculated by TDDFT B3LYP/6-31G(d) method with PCM model (THF) in adiabatic approximation.

The most intriguing property of **pCNBCzoCF<sub>3</sub>** is extremely small  $\Delta E_{\text{ST}}$ . As one can see from Figure 2 both PL and phosphorescence spectra of the solid film of **pCNBCzoCF<sub>3</sub>** are characterized by almost the same peak positions. The PL maximum appears at 477.0 nm (red curve) while the highest energy vibronic sub-band in the phosphorescence spectrum (left-hand shoulder at the green curve) appears at 479.0 nm. These values correspond to  $\Delta E_{\text{ST}}$  value of only 0.011 eV, which is favourable for efficient TADF emission. Such a small  $\Delta E_{\text{ST}}$  value is in complete agreement with our vertical TD DFT calculations (2.768 eV for S<sub>1</sub> and 2.757 eV for T<sub>1</sub>) proving the equivalent  $\Delta E_{\text{ST}}$  value (0.011 eV). We have additionally performed the computations for the  $\Delta E_{\text{ST}}$  value in adiabatic approximation by the direct optimization of S<sub>1</sub> and T<sub>1</sub> excited states within TDDFT/B3LYP/6-31G(d) method. The calculated adiabatic difference between S<sub>1</sub> (2.455 eV) and T<sub>1</sub> (2.447 eV) states

was found to be only 0.008 eV in a complete agreement with “vertical” approximation and experimental value. Moreover, the calculated 0-0 energies for S<sub>1</sub> and T<sub>1</sub> states are even in better agreement with the experimental values than “vertical” energies (Table 1). Here we should note that our  $\Delta E_{ST}$  value is in some inconsistency with the data of Ref.<sup>16</sup> where  $\Delta E_{ST}$  for *p*CNBCzoCF<sub>3</sub> was estimated to be of 0.19 eV. Such mismatch in the singlet-triplet energy splitting values (0.19 eV in Ref. vs. 0.02 eV) originates from the different PL spectra of the solid film of *p*CNBCzoCF<sub>3</sub> recorded at 77 K. The PL spectrum presented in Ref.<sup>16</sup> consists of double emission peaks at 449 and 468 nm in contrast to our data (478 nm). At the same time, the phosphorescence spectra recorded by us and by the authors of Ref.<sup>16</sup> are closely similar (double-peak curve profile with 474 and 489 nm maxima in Ref.<sup>16</sup> vs. 474 and 491 nm in this work). In any case, we believe that the  $\Delta E_{ST}$  value of 0.19 eV reported in Ref.<sup>16</sup> is overestimated since such a high singlet-triplet splitting can not necessitate the pronounced TADF behaviour of *p*CNBCzoCF<sub>3</sub>.

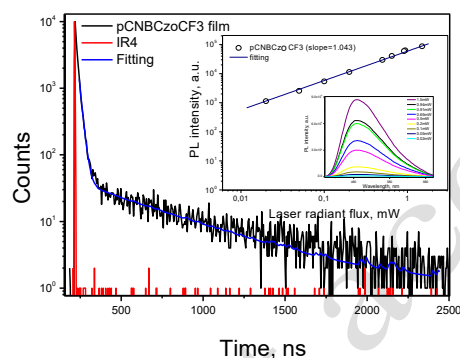


**Figure 4.** Photoluminescence decay curves of vacuum deposited layer of *p*CNBCzoCF<sub>3</sub> in nanosecond time ranges; (insert) the dependence of PL intensity of the layer of *p*CNBCzoCF<sub>3</sub> on laser flux (insert: PL spectra recorded at the different excitation power).

The TADF nature of *p*CNBCzoCF<sub>3</sub> emission was confirmed by PL decay measurements for the neat film of *p*CNBCzoCF<sub>3</sub> (Figure 4). The double exponential law for the PL decay curve of the solid sample of *p*CNBCzoCF<sub>3</sub> was required for fitting ( $\chi^2=1.157$ ) of the decay curve according to the formula  $A+B_1\exp(-t/\tau_1)+B_2\exp(-t/\tau_2)$ . The corresponding PL lifetimes  $\tau_1=17.36$  ns (83 %) and  $\tau_2=503$  ns (17 %) were obtained. The second component ( $\tau_2$ ) is much shorter than that of 8.12  $\mu$ s earlier recorded for the solution *p*CNBCzoCF<sub>3</sub> in toluene.<sup>16</sup> The longer-lived component of the decay can be determined by two effects; one being due to the triplet-triplet annihilation<sup>34</sup>, the other being due to the TADF effect<sup>35</sup>. However, with a linear dependence of PL intensity on laser flux with slope of ca. 1 for the solid layer of *p*CNBCzoCF<sub>3</sub> (Figure 4), this longer-lived component must be attributed to the reverse intersystem crossing process (RISC), proving the TADF nature of PL emission of *p*CNBCzoCF<sub>3</sub>. Additionally, temperature dependences of PL spectra and PL decays were recorded for *p*CNBCzoCF<sub>3</sub> film (Figure S5). The most intensive PL, consisting of both fluorescence and phosphorescence, was observed at 80 K. PL intensity decreased with increasing temperature up to 180K due to phosphorescence quenching. At temperatures higher than 180K, PL intensity started increase. This increase of PL intensity was caused by TADF

### Solid-state ionization potential and charge-transporting properties of the layers of *p*CNBCzoCF<sub>3</sub>

Solid-state ionization potential (IP) of 5.84 eV was recorded for the solid layer of *p*CNBCzoCF<sub>3</sub> by electron photoemission method (Figure 5a). This IP value observed for the vacuum deposited layer of *p*CNBCzoCF<sub>3</sub> was found to be higher than that obtained from the electrochemical measurements (HOMO(CV) of  $-5.41$  eV)<sup>16</sup>. Such disagreement

in the IP values is apparently due to intermolecular interactions of *p*CNBCzoCF<sub>3</sub> molecules that can take place in the solid layers. Having the solid-state IP energy levels of 5.84 eV and the solid-state optical band-gap energy ( $E_g$ ) of ca. 2.92 eV<sup>16</sup>, electron affinity ( $E_A$ ) was calculated as  $E_A = IP - E_g = 2.92$  eV. Therefore, the HOMO and LUMO values of -5.84 and -2.92 eV were used to design OLEDs as they are related to IP and  $E_A$ , respectively.

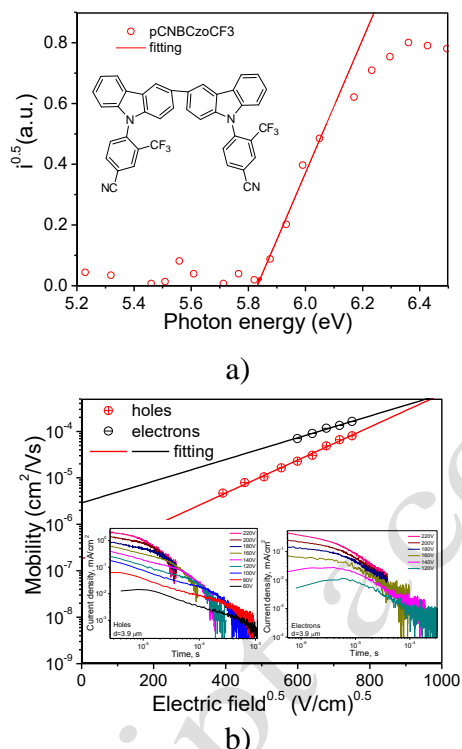


**Figure 5.** (a) Electron photoemission spectrum of the vacuum deposited layer of *p*CNBCzoCF<sub>3</sub> (b) electric field dependencies of hole and electron mobilities and the hole and electron TOF transient curves for *p*CNBCzoCF<sub>3</sub> in log-log scales (inserts).

Charge-transporting properties of *p*CNBCzoCF<sub>3</sub> were studied by time-of-flight (TOF) method taking into account that charge mobility values were not obtained for *p*CNBCzoCF<sub>3</sub> in the previous article.<sup>16</sup> Figure 5b shows electric field dependencies of hole and electron mobilities of the vacuum deposited layer of *p*CNBCzoCF<sub>3</sub>. Bipolar nature of charge transport in was proved by observing transit times for both holes and electrons on the TOF transient curves (Figure 5b, inserts). Twice higher electron mobility of  $1.6 \times 10^{-4}$  cm<sup>2</sup>/(V×s) comparing to hole mobility of  $8 \times 10^{-5}$  cm<sup>2</sup>/(V×s) was observed at electric field of ca.  $5.6 \times 10^5$  V/cm. Such trend of TOF hole and electron mobilities is in good agreement with a trend of hole and electron currents for hole-only and electron-only devices studied in the previous work.<sup>16</sup> This observation can be explained by the introduction of the strong electron-withdrawing meta-positioned CF<sub>3</sub> moieties to the molecules of *p*CNBCzoCF<sub>3</sub>.<sup>16</sup> Charge mobilities observed for *p*CNBCzoCF<sub>3</sub> are comparable to the best known values reported for TADF materials.<sup>36</sup>

### Sky-blue non-doped OLEDs based on *p*CNBCzoCF<sub>3</sub> emission

Three OLEDs A–C were fabricated. The principal schemes of these devices are presented in Figure 6.

EL spectrum of Device A is almost the same as the photoluminescence spectrum of the vacuum spectrum of Device A is almost the same as the photoluminescence spectrum of the vacuum deposited film of *p*CNBCzoCF<sub>3</sub> recorded at ambient conditions (Figure 7). This observation indicates the absence of exciplex-type emission from the interfaces TCTA/*p*CNBCzoCF<sub>3</sub> and *p*CNBCzoCF<sub>3</sub>/BCP. Device A is characterized by a relatively low turn

on voltage of only 3.4 V. The maximum external quantum efficiency, power efficiency and current efficiency of 6.2%, 7.75 lm W<sup>-1</sup> and 15.3 cd A<sup>-1</sup> respectively, were observed for Device A. The maximal brightness reached 29300 cd m<sup>-2</sup> at 15 V (Table 2). Such lighting parameters characterize the emissive properties of the pure *p*CNBCzoCF<sub>3</sub> which can be regarded as promising electroluminescent material for sky-blue OLEDs (Table 2, Figure S1).

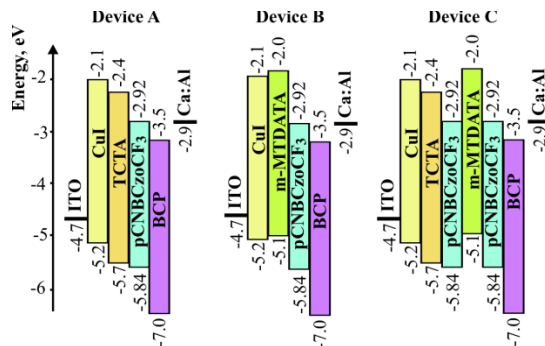


**Figure 6.** The energy diagrams for the devices A–C.

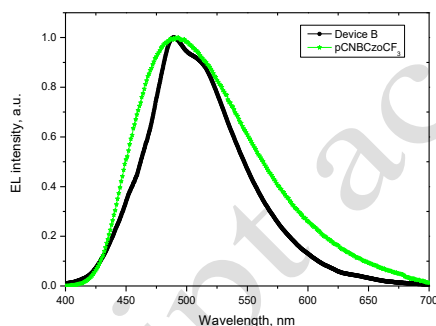


**Figure 7.** Normalized electroluminescence spectrum of Device A vs. photoluminescence spectrum of the solid film of *p*CNBCzoCF<sub>3</sub> recorded at room temperature.

### Orange device exhibiting *m*-MTDATA:*p*CNBCzoCF<sub>3</sub> interface exciplex emission

EL spectrum of Device B coincides with the PL spectrum of the molecular blend *m*-MTDATA:*p*CNBCzoCF<sub>3</sub>. At the same time, both spectra are significantly red shifted with respect of PL spectrum of *p*CNBCzoCF<sub>3</sub> and EL spectrum of Device A (Figure 8). This observation indicates the exciplex formation at the *m*-MTDATA/*p*CNBCzoCF<sub>3</sub> interface which was not observed at the interface TCTA/*p*CNBCzoCF<sub>3</sub>.

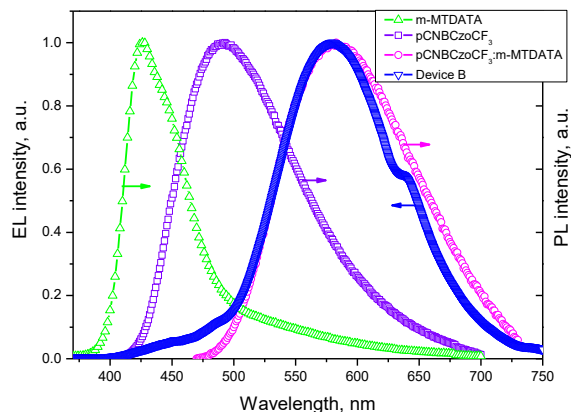


**Figure 8.** Normalized electroluminescence spectrum of Device B vs. photoluminescence spectra of the solid films of *m*-MTDATA, *p*CNBCzoCF<sub>3</sub> and *m*-MTDATA:*p*CNBCzoCF<sub>3</sub> recorded at room temperature.

TADF emission of the layer of *p*CNBCzoCF<sub>3</sub> remains visible as a structureless shoulder in the higher-energy region of 400–500 nm (Figure 8). The lighting characteristics of device **B** are a little better than those of Device **A** (Figure S2.). The chromaticity coordinates of Device **B** lay in the “warm-white” region in contrast the sky-blue emission of Device **A**. Upon the exciplex formation in Device **B** *m*-MTDATA plays the role of electron donor while the bipolar compound *p*CNBCzoCF<sub>3</sub> is an acceptor counterpart. The energy difference of the HOMOs of *m*-MTDATA and *p*CNBCzoCF<sub>3</sub> is of 0.45 eV, while that for the LUMO levels is of 0.52 eV (Figure 6). Due to that mismatch in the HOMO and LUMO energy levels cross-coupling of holes and electrons occurs at the interface *m*-MTDATA/*p*CNBCzoCF<sub>3</sub> and as a result intense exciplex-type broad emission is observed in the region of 500–750 nm (Figure 8).

PL lifetimes of  $\tau_1=105$  ns (80 %) and  $\tau_2=458$  ns (20 %) were obtained by fitting the PL decay curve the solid-state mixture *m*-MTDATA:*p*CNBCzoCF<sub>3</sub> with the double exponential law (Figure 9). In addition, the linear dependence of PL intensity on the laser flux (with a slope of ca. 1) was recorded for the studied solid-state mixture similarly to that observed for a film of *p*CNBCzoCF<sub>3</sub> (Figure 9, insert). Therefore, the TADF nature of *m*-MTDATA:*p*CNBCzoCF<sub>3</sub> exciplex emission can be expected as for the exciplexes published before<sup>36,37</sup>.

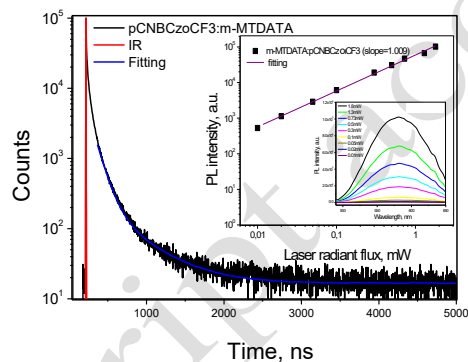
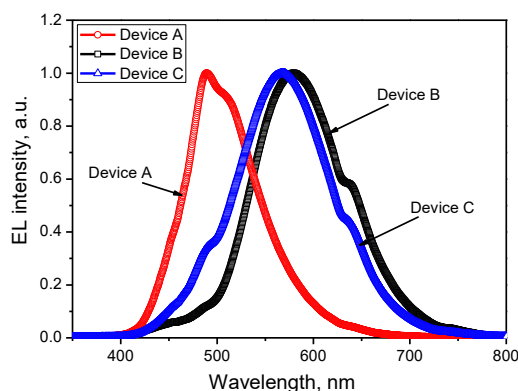


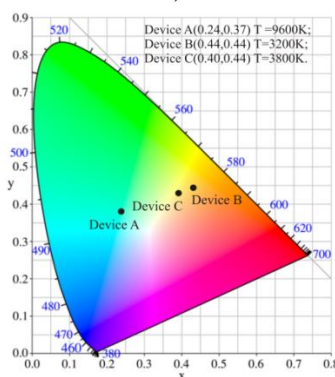
**Figure 9.** Photoluminescence decay curve and the dependence of PL intensity on laser flux for the film of the mixture *m*-MTDATA:*p*CNBCzoCF<sub>3</sub> (insert: PL spectra recorded at the different power excitation).

### “Warm-white” device based on both *p*CNBCzoCF<sub>3</sub> TADF emission and on *m*-MTDATA:*p*CNBCzoCF<sub>3</sub> interface exciplex emission

Combining devices **A** and **B** within one OLED we fabricated highly-efficient device **C** with warm-white emission colour. EL spectrum of Device **C** represents the superposition of EL spectra of Devices **A** and **B**. The additional *p*CNBCzoCF<sub>3</sub> layer (adjacent to that of TCTA) provides the enhancement of the short-wavelength emission which originates from the TADF emission of *p*CNBCzoCF<sub>3</sub>. As a result, EL spectrum of Device **C** covers the region from 450 to 750 nm (Figure 10).



a)



b)

**Figure 10.** Normalized EL spectra of devices A–C (a) and their CIE1976 chromaticity coordinates with the corresponding values of colour temperature (b).

**Table 2.** Lighting characteristics of devices A–C.

Device	$V_{on}$ (V)	Max. brightness at 15 V ( $\text{cd}/\text{m}^2$ )	Max. current (mA)	Max. power (mW)	Max. external efficiency (%)	At 1000 $\text{Cd}/\text{m}^2$			Colour coordi nate (CIE 1976)
						Current (mA)	Power (mW)	External efficiency (%)	
<b>A</b>	3.4	293	15.	10.	6.3	15.	7.7	6.2	(0.24,0 .37)
	4.0	00	5	3		3	5		
<b>B</b>	2.8	345	18.	12.	9.4	18.	9.4	9.3	(0.44,0 .44)
	8.0	00	2	1		0	6		
<b>C</b>	6.4	409	53.	19.	18.	46.	10.	17.	(0.40,0 .44)
	8.0	00	8	3	8	2	6	0	

The lighting characteristics of devices A–C are presented in the Table 2. Device C demonstrates outstanding lighting characteristics comparing with those of Devices A and B. These characteristics were achieved by the rational combination of green-blue TADF emission of *p*CNBCzoCF<sub>3</sub> layer with the orange exiplex emission of the *m*-MTDATA/*p*CNBCzoCF<sub>3</sub> interface within the single OLED (Figure S3). The special feature of Device C (as well as of Device B) is the absence of a high-energy emission component in its EL

spectrum. Therefore, the EL of the fabricated devices **B** and **C** is harmless for the human eye. Particularly, the colour temperatures of Devices **B** and **C** were estimated as 3200 and 3800 K, respectively, that are close to the common standards (2700–3500 K) for the warm-white compact fluorescent and LED lamps<sup>38</sup>. In addition, the devices **B** and **C** exhibiting warm white electroluminescence were characterized by 60 of colour rendering index (CRI) which is satisfied value of white light sources for lighting applications. We should also note that the efficiencies of Devices **B** and **C** are comparable (Figure S4) (or even higher) to those of iridium-based warm-white phosphorescent OLEDs<sup>3</sup>.

## Conclusions

In the present work we studied 4,4'-(9H,9'H-[3,3'-bicarbazole]-9,9'-diyl)bis(3-(trifluoromethyl)benzotrile) (*p*CNBCzoCF<sub>3</sub>) which demonstrates clear TADF depending on temperature. The material is characterized by the singlet-triplet energy splitting of only 0.011 eV as estimated both by experimental measurements and TDDFT calculations. We used *p*CNBCzoCF<sub>3</sub> as a green-blue emitter and also as an exciplex-forming material for OLED fabrication. The simplest green-blue device based on pure electroluminescence of *p*CNBCzoCF<sub>3</sub> was shown to exhibit good lighting characteristics with the maximal external quantum efficiency of 6.2%. In order to improve efficiency of the device and to extend its EL spectrum over the whole visible range, we combined green-blue TADF-type electroluminescence of *p*CNBCzoCF<sub>3</sub> with exciplex-type emission from the *m*-MTDATA/*p*CNBCzoCF<sub>3</sub> interface. The device obtained was characterized by the warm-white emission and by outstanding lighting characteristics: brightness of 40900 Cd/m<sup>2</sup> (at 15 V), current efficiency of 53.8 Cd/A and power efficiency of 19.3 lm/W, external quantum efficiency of 18.8 %.

## Results and discussion

### Spectroscopic characterization of *p*CNBCzoCF<sub>3</sub>

The experimental absorption spectrum of the solution of *p*CNBCzoCF<sub>3</sub> in THF recorded at ambient conditions is presented in Figure 2 (orange line). For the comparison, the theoretical spectrum simulated by the TD DFT method accounting for the PCM model is shown in Figure 2 (blue line). The first singlet electronic transition in the spectrum of *p*CNBCzoCF<sub>3</sub> is reflected at 447.6 nm (Table 1) but appears only weakly in the experimental and theoretically simulated spectra. Accounting the fact that *p*CNBCzoCF<sub>3</sub> is a  $\sigma$ -bond coupled dimer of 4-(9H-carbazol-9-yl)-3-(trifluoromethyl)benzotrile the first singlet and triplet excited states are almost doubly degenerated. Due to the absence of strict symmetry constraints the S<sub>1</sub> and S<sub>2</sub> states are split by 0.2 nm in our calculations and the T<sub>1</sub> and T<sub>2</sub> states are split by 0.3 nm (Table 1). As it can be seen from Figure 3 both S<sub>1</sub> and S<sub>2</sub> states of *p*CNBCzoCF<sub>3</sub> are of charge transfer (CT) type and these transitions correspond to electron density moving from 3-(trifluoromethyl)benzotrile moieties to carbazole units. It is a general rule that CT transitions are characterized by a very weak intensity and also are sensitive to the influence of a solvent.<sup>33</sup> Indeed, the energy of S<sub>1</sub> and S<sub>2</sub> states increase significantly in THF environment (2.77 eV) comparing with the vacuum approximation (2.64 eV).

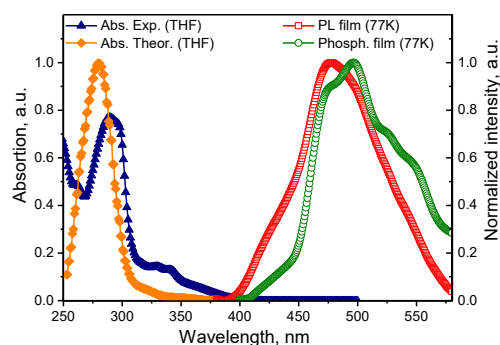


**Figure 2.** Absorption and emission spectra of *p*CN*BCzo*CF<sub>3</sub>.

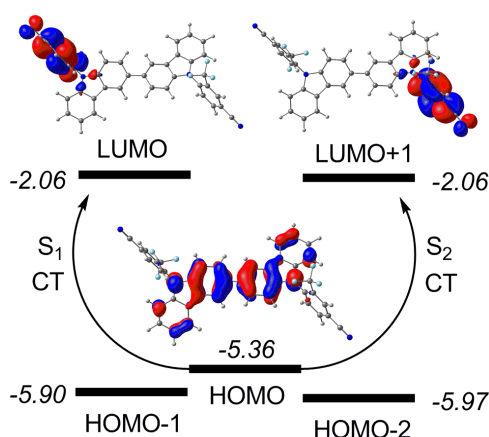


**Figure 3.** MOs levels diagram for *p*CN*BCzo*CF<sub>3</sub> (italic numbers are the MOs energies in eV).

Due to weak intensity of the  $S_0 \rightarrow S_1$  transition the photoluminescence quantum yield of *p*CN*BCzo*CF<sub>3</sub> was measured as 19.3 and 20 % for the THF solution and solid film state, respectively, indicating the dominant role of non-radiative quenching processes in the deactivation of the first excited singlet state.

The long-wavelength shoulder in the absorption spectrum of *p*CN*BCzo*CF<sub>3</sub> solution (310–370 nm) can be assigned to the manifold of weak singlet-singlet electronic transitions  $S_0 \rightarrow S_{3-14}$ . Among them the electronic transitions into  $S_5$  and  $S_{12}$  states are the most intense (Table 1). The high-intensity absorption band at ca. 290 nm corresponds to two electronic transitions  $S_0 \rightarrow S_{15}$  and  $S_0 \rightarrow S_{20}$  from the frontier occupied MOs into the high-lying unoccupied orbitals.

**Table 1.** Assignment of absorption spectrum of *p*CN*BCzo*CF<sub>3</sub> together with estimations of  $S_1$  and  $T_1$  energies.

State	$\lambda_{\text{theor.}}^{\text{abs.}}$ , nm	$\lambda_{\text{exp.}}^{\text{abs.}}$ , nm	$E_{\text{exp.}}/E_t$ heor., eV	$f$	Assignment
$T_1$	449.4	-	2.64 <sup>a</sup> /2 .586 <sup>c</sup> /2 .757 <sup>e</sup>	0	HOMO → LUMO (78%)



presented in Ref.<sup>16</sup> consists of double emission peaks at 449 and 468 nm in contrast to our data (478 nm). At the same time, the phosphorescence spectra recorded by us and by the authors of Ref.<sup>16</sup> are closely similar (double-peak curve profile with 474 and 489 nm maxima in Ref.<sup>16</sup> vs. 474 and 491 nm in this work). In any case, we believe that the  $\Delta E_{ST}$  value of 0.19 eV reported in Ref.<sup>16</sup> is overestimated since such a high singlet-triplet splitting can not necessitate the pronounced TADF behaviour of *p*CNBCzoCF<sub>3</sub>.

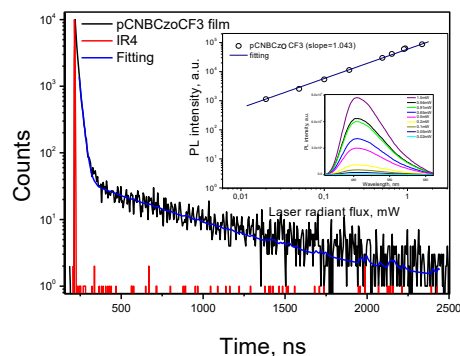


**Figure 4.** Photoluminescence decay curves of vacuum deposited layer of *p*CNBCzoCF<sub>3</sub> in nanosecond time ranges; (insert) the dependence of PL intensity of the layer of *p*CNBCzoCF<sub>3</sub> on laser flux (insert: PL spectra recorded at the different excitation power).

The TADF nature of *p*CNBCzoCF<sub>3</sub> emission was confirmed by PL decay measurements for the neat film of *p*CNBCzoCF<sub>3</sub> (Figure 4). The double exponential law for the PL decay curve of the solid sample of *p*CNBCzoCF<sub>3</sub> was required for fitting ( $\chi^2=1.157$ ) of the decay curve according to the formula  $A+B_1\exp(-t/\tau_1)+B_2\exp(-t/\tau_2)$ . The corresponding PL lifetimes  $\tau_1=17.36$  ns (83 %) and  $\tau_2=503$  ns (17 %) were obtained. The second component ( $\tau_2$ ) is much shorter than that of 8.12  $\mu$ s earlier recorded for the solution *p*CNBCzoCF<sub>3</sub> in toluene.<sup>16</sup> The longer-lived component of the decay can be determined by two effects; one being due to the triplet-triplet annihilation<sup>34</sup>, the other being due to the TADF effect<sup>35</sup>. However, with a linear dependence of PL intensity on laser flux with slope of ca. 1 for the solid layer of *p*CNBCzoCF<sub>3</sub> (Figure 4), this longer-lived component must be attributed to the reverse intersystem crossing process (RISC), proving the TADF nature of PL emission of *p*CNBCzoCF<sub>3</sub>. Additionally, temperature dependences of PL spectra and PL decays were recorded for *p*CNBCzoCF<sub>3</sub> film (Figure S5). The most intensive PL, consisting of both fluorescence and phosphorescence, was observed at 80 K. PL intensity decreased with increasing temperature up to 180K due to phosphorescence quenching. At temperatures higher than 180K, PL intensity started increase. This increase of PL intensity was caused by TADF

### Solid-state ionization potential and charge-transporting properties of the layers of *p*CNBCzoCF<sub>3</sub>

Solid-state ionization potential (IP) of 5.84 eV was recorded for the solid layer of *p*CNBCzoCF<sub>3</sub> by electron photoemission method (Figure 5a). This IP value observed for the vacuum deposited layer of *p*CNBCzoCF<sub>3</sub> was found to be higher than that obtained from the electrochemical measurements (HOMO(CV) of  $-5.41$  eV)<sup>16</sup>. Such disagreement in the IP values is apparently due to intermolecular interactions of *p*CNBCzoCF<sub>3</sub> molecules that can take place in the solid layers. Having the solid-state IP energy levels of 5.84 eV and the solid-state optical band-gap energy ( $E_g$ ) of ca. 2.92 eV<sup>16</sup>, electron affinity ( $E_A$ ) was calculated as  $E_A = IP - E_g = 2.92$  eV. Therefore, the HOMO and LUMO values of -5.84 and -2.92 eV were used to design OLEDs as they are related to IP and  $E_A$ , respectively.

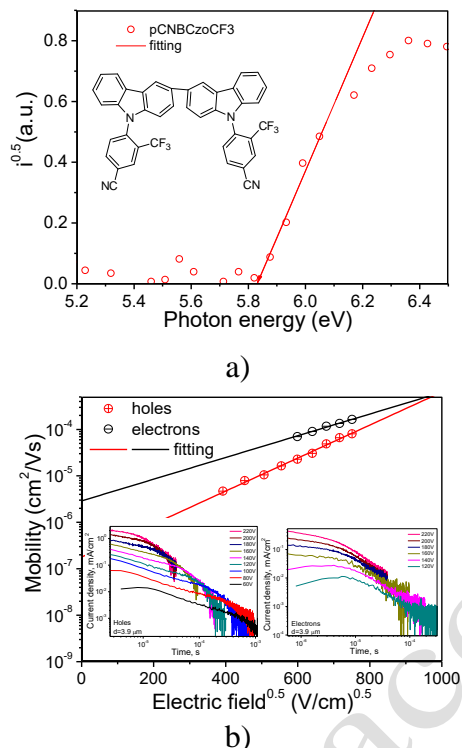


**Figure 5.** (a) Electron photoemission spectrum of the vacuum deposited layer of *pCNBCzoCF<sub>3</sub>* (b) electric field dependencies of hole and electron mobilities and the hole and electron TOF transient curves for *pCNBCzoCF<sub>3</sub>* in log-log scales (inserts).

Charge-transporting properties of *pCNBCzoCF<sub>3</sub>* were studied by time-of-flight (TOF) method taking into account that charge mobility values were not obtained for *pCNBCzoCF<sub>3</sub>* in the previous article.<sup>16</sup> Figure 5b shows electric field dependencies of hole and electron mobilities of the vacuum deposited layer of *pCNBCzoCF<sub>3</sub>*. Bipolar nature of charge transport in was proved by observing transit times for both holes and electrons on the TOF transient curves (Figure 5b, inserts). Twice higher electron mobility of  $1.6 \times 10^{-4} \text{ cm}^2/(\text{V} \times \text{s})$  comparing to hole mobility of  $8 \times 10^{-5} \text{ cm}^2/(\text{V} \times \text{s})$  was observed at electric field of ca.  $5.6 \times 10^5 \text{ V/cm}$ . Such trend of TOF hole and electron mobilities is in good agreement with a trend of hole and electron currents for hole-only and electron-only devices studied in the previous work.<sup>16</sup> This observation can be explained by the introduction of the strong electron-withdrawing meta-positioned  $\text{CF}_3$  moieties to the molecules of *pCNBCzoCF<sub>3</sub>*.<sup>16</sup> Charge mobilities observed for *pCNBCzoCF<sub>3</sub>* are comparable to the best known values reported for TADF materials.<sup>36</sup>

### Sky-blue non-doped OLEDs based on *pCNBCzoCF<sub>3</sub>* emission

Three OLEDs A–C were fabricated. The principal schemes of these devices are presented in Figure 6.

EL spectrum of Device A is almost the same as the photoluminescence spectrum of the vacuum deposited film of *pCNBCzoCF<sub>3</sub>* recorded at ambient conditions (Figure 7). This observation indicates the absence of exciplex-type emission from the interfaces TCTA/*pCNBCzoCF<sub>3</sub>* and *pCNBCzoCF<sub>3</sub>*/BCP. Device A is characterized by a relatively low turn on voltage of only 3.4 V. The maximum external quantum efficiency, power efficiency and current efficiency of 6.2%,  $7.75 \text{ lm W}^{-1}$  and  $15.3 \text{ cd A}^{-1}$  respectively, were observed for Device A. The maximal brightness reached  $29300 \text{ cd m}^{-2}$  at 15 V (Table 2). Such lighting parameters characterize the emissive properties of the pure *pCNBCzoCF<sub>3</sub>* which can be

regarded as promising electroluminescent material for sky-blue OLEDs (Table 2, Figure S1).

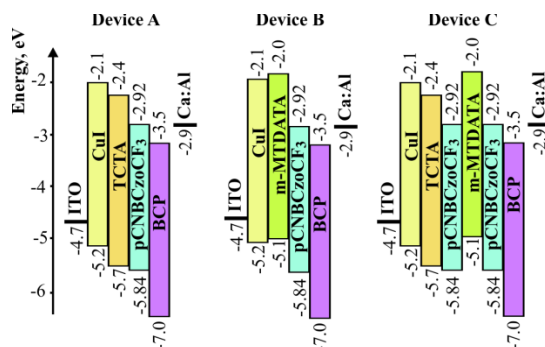


**Figure 6.** The energy diagrams for the devices A–C.

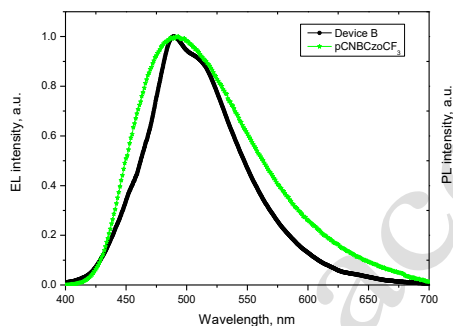


**Figure 7.** Normalized electroluminescence spectrum of Device A vs. photoluminescence spectrum of the solid film of  $p\text{CNBCzoCF}_3$  recorded at room temperature.

### Orange device exhibiting $m\text{-MTDATA}:p\text{CNBCzoCF}_3$ interface exciplex emission

EL spectrum of Device B coincides with the PL spectrum of the molecular blend  $m\text{-MTDATA}:p\text{CNBCzoCF}_3$ . At the same time, both spectra are significantly red shifted with respect of PL spectrum of  $p\text{CNBCzoCF}_3$  and EL spectrum of Device A (Figure 8). This observation indicates the exciplex formation at the  $m\text{-MTDATA}/p\text{CNBCzoCF}_3$  interface which was not observed at the interface  $\text{TCTA}/p\text{CNBCzoCF}_3$ .

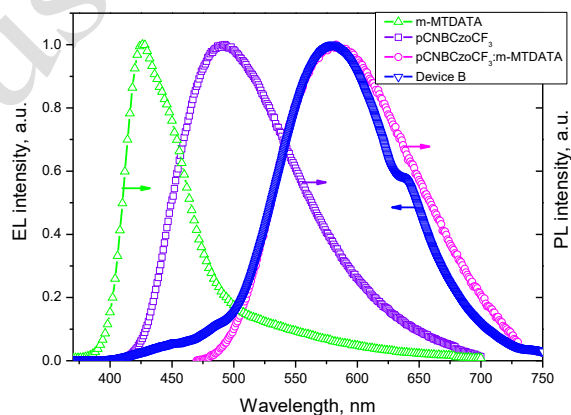
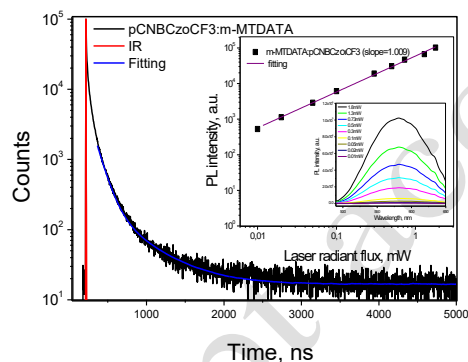


**Figure 8.** Normalized electroluminescence spectrum of Device B vs. photoluminescence spectra of the solid films of  $m\text{-MTDATA}$ ,  $p\text{CNBCzoCF}_3$  and  $m\text{-MTDATA}:p\text{CNBCzoCF}_3$  recorded at room temperature.

TADF emission of the layer of  $p\text{CNBCzoCF}_3$  remains visible as a structureless shoulder in the higher-energy region of 400-500 nm (Figure 8). The lighting characteristics of device

**B** are a little better than those of Device **A** (Figure S2.). The chromaticity coordinates of Device **B** lay in the “warm-white” region in contrast the sky-blue emission of Device **A**. Upon the exciplex formation in Device **B** *m*-MTDATA plays the role of electron donor while the bipolar compound *p*CNBCzoCF<sub>3</sub> is an acceptor counterpart. The energy difference of the HOMOs of *m*-MTDATA and *p*CNBCzoCF<sub>3</sub> is of 0.45 eV, while that for the LUMO levels is of 0.52 eV (Figure 6). Due to that mismatch in the HOMO and LUMO energy levels cross-coupling of holes and electrons occurs at the interface *m*-MTDATA/*p*CNBCzoCF<sub>3</sub> and as a result intense exciplex-type broad emission is observed in the region of 500–750 nm (Figure 8).

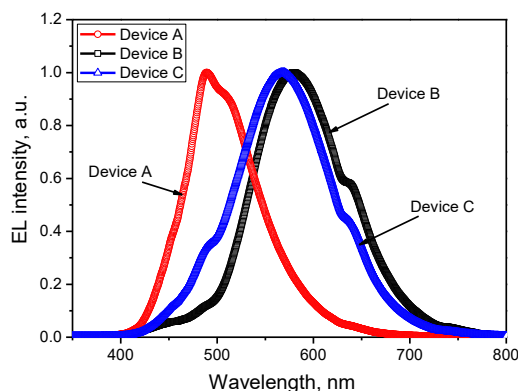
PL lifetimes of  $\tau_1=105$  ns (80 %) and  $\tau_2=458$  ns (20 %) were obtained by fitting the PL decay curve the solid-state mixture *m*-MTDATA:*p*CNBCzoCF<sub>3</sub> with the double exponential law (Figure 9). In addition, the linear dependence of PL intensity on the laser flux (with a slope of ca. 1) was recorded for the studied solid-state mixture similarly to that observed for a film of *p*CNBCzoCF<sub>3</sub> (Figure 9, insert). Therefore, the TADF nature of *m*-MTDATA:*p*CNBCzoCF<sub>3</sub> exciplex emission can be expected as for the exciplexes published before<sup>36,37</sup>.



**Figure 9.** Photoluminescence decay curve and the dependence of PL intensity on laser flux for the film of the mixture *m*-MTDATA:*p*CNBCzoCF<sub>3</sub> (insert: PL spectra recorded at the different power excitation).

### “Warm-white” device based on both *p*CNBCzoCF<sub>3</sub> TADF emission and on *m*-MTDATA:*p*CNBCzoCF<sub>3</sub> interface exciplex emission

Combining devices **A** and **B** within one OLED we fabricated highly-efficient device **C** with warm-white emission colour. EL spectrum of Device **C** represents the superposition of EL spectra of Devices **A** and **B**. The additional *p*CNBCzoCF<sub>3</sub> layer (adjacent to that of TCTA) provides the enhancement of the short-wavelength emission which originates from the TADF emission of *p*CNBCzoCF<sub>3</sub>. As a result, EL spectrum of Device **C** covers the region from 450 to 750 nm (Figure 10).



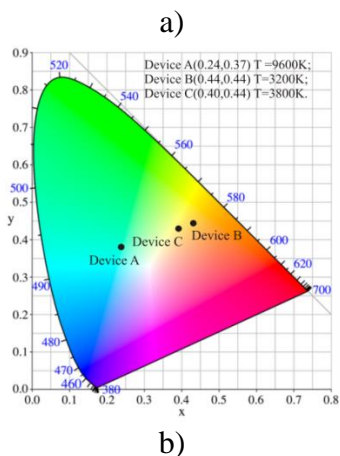


**Figure 10.** Normalized EL spectra of devices **A–C** (a) and their CIE1976 chromaticity coordinates with the corresponding values of colour temperature (b).

**Table 2.** Lighting characteristics of devices **A–C**.

Device	$V_{on}$ (V)	Max. brightness at 15 V ( $\text{Cd}/\text{m}^2$ )	Max. current ( $\text{mA}/\text{A}$ )	Max. power ( $\text{W}/\text{W}$ )	Max. external efficiency (%)	At 1000 $\text{Cd}/\text{m}^2$			Colour coordinate (CIE 1976)
						Current (mA)	Power (W)	External efficiency (%)	
<b>A</b>	3.	293	15.	10.	6.3	15.	7.7	6.2	(0.24,0
	4	00	5	3	6.3	3	5	6.2	.37)
<b>B</b>	2.	345	18.	12.	9.4	18.	9.4	9.3	(0.44,0
	8	00	2	1	9.4	0	6	9.3	.44)
<b>C</b>	6.	409	53.	19.	18.	46.	10.	17.	(0.40,0
	8	00	8	3	8	2	6	0	.44)

The lighting characteristics of devices **A–C** are presented in the Table 2. Device **C** demonstrates outstanding lighting characteristics comparing with those of Devices **A** and **B**. These characteristics were achieved by the rational combination of green-blue TADF emission of  $p\text{CNBCzoCF}_3$  layer with the orange exiplex emission of the  $m\text{-MTDATA}/p\text{CNBCzoCF}_3$  interface within the single OLED (Figure S3). The special feature of Device **C** (as well as of Device **B**) is the absence of a high-energy emission component in its EL spectrum. Therefore, the EL of the fabricated devices **B** and **C** is harmless for the human eye. Particularly, the colour temperatures of Devices **B** and **C** were estimated as 3200 and 3800 K, respectively, that are close to the common standards (2700–3500 K) for the warm-white compact fluorescent and LED lamps<sup>38</sup>. In addition, the devices **B** and **C** exhibiting warm white electroluminescence were characterized by 60 of colour rendering index (CRI) which is satisfied value of white light sources for lighting applications. We should also note that the efficiencies of Devices **B** and **C** are comparable (Figure S4) (or even higher) to those of iridium-based warm-white phosphorescent OLEDs<sup>3</sup>.

## Conclusions

In the present work we studied 4,4'-(9H,9'H-[3,3'-bicarbazole]-9,9'-diyl)bis(3-(trifluoromethyl)benzotrile) (*p*CNBCzoCF<sub>3</sub>) which demonstrates clear TADF depending on temperature. The material is characterized by the singlet-triplet energy splitting of only 0.011 eV as estimated both by experimental measurements and TDDFT calculations. We used *p*CNBCzoCF<sub>3</sub> as a green-blue emitter and also as an exciplex-forming material for OLED fabrication. The simplest green-blue device based on pure electroluminescence of *p*CNBCzoCF<sub>3</sub> was shown to exhibit good lighting characteristics with the maximal external quantum efficiency of 6.2%. In order to improve efficiency of the device and to extend its EL spectrum over the whole visible range, we combined green-blue TADF-type electroluminescence of *p*CNBCzoCF<sub>3</sub> with exciplex-type emission from the *m*-MTDATA/*p*CNBCzoCF<sub>3</sub> interface. The device obtained was characterized by the warm-white emission and by outstanding lighting characteristics: brightness of 40900 Cd/m<sup>2</sup> (at 15 V), current efficiency of 53.8 Cd/A and power efficiency of 19.3 lm/W, external quantum efficiency of 18.8 %.

### Notes and references

- 1 J.-H. Jou, R.-Z. Wu, H.-H. Yu, C.-J. Li, Y.-C. Jou, S.-H. Peng, Y.-L. Chen, C.-T. Chen, S.-M. Shen, P. Joers and C.-Y. Hsieh, Artificial Dusk-Light Based on Organic Light Emitting Diodes, *ACS Photonics*, 2014, **1**, 27–31.
- 2 J.-H. Jou, M.-C. Tang, P.-C. Chen, Y.-S. Wang, S.-M. Shen, B.-R. Chen, C.-H. Lin, W.-B. Wang, S.-H. Chen, C.-T. Chen, F.-Y. Tsai, C.-W. Wang, C.-C. Chen and C.-C. Wang, Organic light-emitting diode-based plausibly physiologically-friendly low color-temperature night light, *Org. Electron.*, 2012, **13**, 1349–1355.
- 3 V. Cherpak, P. Stakhira, B. Minaev, G. Baryshnikov, E. Stromylo, I. Helzhynskyy, M. Chapran, D. Volyniuk, D. Tomkute-Luksiene, T. Malinauskas, V. Getautis, A. Tomkeviciene, J. Simokaitiene and J. V. Grazulevicius, Efficient “Warm-White” OLEDs based on the phosphorescent bis-cyclometalated iridium(III) complex, *J. Phys. Chem. C*, 2014, **118**, 11271–11278.
- 4 Y.-L. Chang, Y. Song, Z. Wang, M. G. Helander, J. Qiu, L. Chai, Z. Liu, G. D. Scholes and Z. Lu, Highly Efficient Warm White Organic Light-Emitting Diodes by Triplet Exciton Conversion, *Adv. Funct. Mater.*, 2013, **23**, 705–712.
- 5 D. Zhang, L. Duan, Y. Li, D. Zhang and Y. Qiu, Highly efficient and color-stable hybrid warm white organic light-emitting diodes using a blue material with thermally activated delayed fluorescence, *J. Mater. Chem. C*, 2014, **2**, 8191–8197.
- 6 J.-H. Lee, S.-H. Cheng, S.-J. Yoo, H. Shin, J.-H. Chang, C.-I. Wu, K.-T. Wong and J.-J. Kim, An Exciplex Forming Host for Highly Efficient Blue Organic Light Emitting Diodes with Low Driving Voltage, *Adv. Funct. Mater.*, 2015, **25**, 361–366.
- 7 Y.-H. Chen, K.-C. Tang, Y.-T. Chen, J.-Y. Shen, Y.-S. Wu, S.-H. Liu, C.-S. Lee, C.-H. Chen, T.-Y. Lai, S.-H. Tung, R.-J. Jeng, W.-Y. Hung, M. Jiao, C.-C. Wu and P.-T. Chou, Insight into the mechanism and outcoupling enhancement of excimer-associated white light generation, *Chem. Sci.*, 2016, **7**, 3556–3563.
- 8 M. Jiao, C.-Y. Lu, W.-K. Lee, C.-Y. Chen and C.-C. Wu, Simple Planar Indium-Tin-Oxide-Free Organic Light-Emitting Devices with Nearly 39% External Quantum Efficiency, *Adv. Opt. Mater.*, 2016, **4**, 365–370.
- 9 J.-J. Huang, Y.-H. Hung, P.-L. Ting, Y.-N. Tsai, H.-J. Gao, T.-L. Chiu, J.-H. Lee, C.-L. Chen, P.-T. Chou and M. Leung, Orthogonally Substituted Benzimidazole-Carbazole Benzene As Universal Hosts for Phosphorescent Organic Light-Emitting Diodes, *Org. Lett.*, 2016, **18**, 672–675.
- 10 G. H. Lee and Y. S. Kim, High-efficiency diphenylsulfon derivative-based organic light-emitting diode exhibiting thermally-activated delayed fluorescence, *J. Korean Phys. Soc.*, 2016, **69**, 398–401.
- 11 G. Valchanov, A. Ivanova, A. Tadjer, D. Chercka and M. Baumgarten, Understanding the Fluorescence of TADF Light-Emitting Dyes, *J. Phys. Chem. A*, 2016, **120**, 6944–6955.
- 12 Y. Danyliv, R. Lytvyn, D. Volyniuk, O. Bezikonnyi, I. Hladka, J.V. Grazulevicius. Derivatives of carbazole and chloropyridine exhibiting aggregation induced emission enhancement and deep-blue delayed fluorescence. *Dye. Pigment.*, 2018, **149**, 588–596.
- 13 H. Uoyama, K. Goushi, K. Shizu, H. Nomura and C. Adachi, Highly efficient organic light-emitting diodes from delayed fluorescence, *Nature*, 2012, **492**, 234–238.
- 14 T. Serevičius, T. Nakagawa, M.-C. Kuo, S.-H. Cheng, K.-T. Wong, C.-H. Chang, R. C. Kwong, S. Xia and C. Adachi, Enhanced electroluminescence based on thermally activated

delayed fluorescence from a carbazole–triazine derivative, *Phys. Chem. Chem. Phys.*, 2013, **15**, 15850.

15 P. L. Santos, J. S. Ward, P. Data, A. S. Batsanov, M. R. Bryce, F. B. Dias and A. P. Monkman, Engineering the singlet–triplet energy splitting in a TADF molecule, *J. Mater. Chem. C*, 2016, **4**, 3815–3824.

16 X. Cao, J. Hu, Y. Tao, W. Yuan, J. Jin, X. Ma, X. Zhang and W. Huang, Alkyl effects on the optoelectronic properties of bicarbazole/ cyanobenzene hybrid host materials: Double delayed fluorescent host/ dopant systems in solution-processed OLEDs, *Dye. Pigment.*, 2017, **136**, 543–552.

17 E. K. U. Gross, C. A. Ullrich and U. J. Gossmann, Springer, Boston, MA, 1995, pp. 149–171.

18 A. D. Becke, Density-functional exchange-energy approximation with correct asymptotic behavior, *Phys. Rev. A*, 1988, **38**, 3098–3100.

19 C. Lee, W. Yang and R. G. Parr, Development of the Colle-Salvetti correlation-energy formula into a functional of the electron density, *Phys. Rev. B*, 1988, **37**, 785–789.

20 M. M. Francl, W. J. Pietro, W. J. Hehre, J. S. Binkley, M. S. Gordon, D. J. DeFrees and J. A. Pople, Self-consistent molecular orbital methods. XXIII. A polarization-type basis set for second-row elements, *J. Chem. Phys.*, 1982, **77**, 3654–3665.

21 S. M. E. S. J. Tomasi, Electrostatic interaction of a solute with a continuum. A direct utilization of AB initio molecular potentials for the prevision of solvent effects, *Chem. Phys.*, 1981, **55**, 117–129.

22 X. Zhan, C. Risko, F. Amy, C. Chan, W. Zhao, S. Barlow, A. Kahn and S. R. M. Jean-Luc Brédas, Electron Affinities of 1,1-Diaryl-2,3,4,5-tetraphenylsiloles: Direct Measurements and Comparison with Experimental and Theoretical Estimates, *J. Am. Chem. Soc.*, 2005, **127**, 9021–9029.

23 Y. Qiao, Z. Wei, C. Risko, H. Li, J.-L. Brédas, W. Xu and D. Zhu, Synthesis, experimental and theoretical characterization, and field-effect transistor properties of a new class of dibenzothiophene derivatives: From linear to cyclic architectures, *J. Mater. Chem.*, 2012, **22**, 1313–1325.

24 B. R. Kaafarani, A. O. El-Ballouli, R. Trattnig, A. Fonari, S. Sax, B. Wex, C. Risko, R. S. Khayzer, S. Barlow, D. Patra, T. V. Timofeeva, E. J. W. List, J.-L. Brédas and S. R. Marder, Bis(carbazolyl) derivatives of pyrene and tetrahydropyrene: synthesis, structures, optical properties, electrochemistry, and electroluminescence, *J. Mater. Chem. C*, 2013, **1**, 1638.

25 P. Stakhira, V. Cherpak, D. Volynyuk, F. Ivastchysyn, Z. Hotra, V. Tataryn and G. Luka, Characteristics of organic light emitting diodes with copper iodide as injection layer, *Thin Solid Films*, 2010, **518**, 7016–7018.

26 M.-H. Tsai, H.-W. Lin, H.-C. Su, T.-H. Ke, C.-c. Wu, F.-C. Fang, Y.-L. Liao, K.-T. Wong and C.-I. Wu, Highly Efficient Organic Blue Electrophosphorescent Devices Based on 3,6-Bis(triphenylsilyl)carbazole as the Host Material, *Adv. Mater.*, 2006, **18**, 1216–1220.

27 Y. Qian, G. Xie, S. Chen, Z. Liu, Y. Ni, X. Zhou, L. Xie, J. Liang, Y. Zhao, M. Yi, Y. Zhao, W. Wei and W. Huang, A new spiro[fluorene-9,9'-xanthene]-based host material possessing no conventional hole- and electron-transporting units for efficient and low voltage blue PHOLED via simple two-step synthesis, *Org. Electron.*, 2012, **13**, 2741–2746.

28 E. Angioni, M. Chapran, K. Ivaniuk, N. Kostiv, V. Cherpak, P. Stakhira, A. Lazauskas, S. Tamulevicius, D. Volyniuk, N. J. Findlay, T. Tuttle, J. V. Grazulevicius and P. J. Skabara, A single emitting layer white OLED based on exciplex interface emission, *J. Mater. Chem. C*, 2016, **4**, 3851–3856.

29 C.-C. Wu, Y.-T. Lin, K.-T. Wong, R.-T. Chen and Y.-Y. Chien, Efficient Organic Blue-Light-Emitting Devices with Double Confinement on Terfluorenes with Ambipolar Carrier Transport Properties, *Adv. Mater.*, 2004, **16**, 61–65.

30 D. Volyniuk, V. Cherpak, P. Stakhira, B. Minaev, G. Baryshnikov, M. Chapran, A. Tomkeviciene, J. Keruckas and J. V. Grazulevicius, Highly Efficient Blue Organic Light-Emitting Diodes Based on Intermolecular Triplet–Singlet Energy Transfer, *J. Phys. Chem. C*, 2013, **117**, 22538–22544.

31 a) E. Miyamoto, Y. Yamaguchi, M. Yokoyama. *Electrophotography*, 1989, **28**, 364–370. b) N. A. Kukhta, D. Volyniuk, L. Peciulyte, J. Ostrauskaite, G. Juska and J. V. Grazulevicius, Structure-property relationships of star-shaped blue-emitting charge-transporting 1,3,5-triphenylbenzene derivatives, *Dye. Pigment.*, 2015, **117**, 122–132.

32 V. Mimaite, J. V. Grazulevicius, R. Laurinaviciute, D. Volyniuk, V. Jankauskas and G. Sini, Can hydrogen bonds improve the hole-mobility in amorphous organic semiconductors? Experimental and theoretical insights, *J. Mater. Chem. C*, 2015, **3**, 11660–11674.

- 33 a) F.B. Dias, K.N. Bourdakos, V. Jankus, K.C. Moss, K.T. Kamtekar, V. Bhalla, J. Santos, M.R. Bryce, A.P. Monkman. Triplet harvesting with 100% efficiency by way of thermally activated delayed fluorescence in charge transfer oled emitters. *Adv. Mater.*, 2013, **25**, 3707–3714. b) N.A. Kukhta, D.A. da Silva Filho, D. Volyniuk, J.V. Grazulevicius, G. Sini. Can fluorenone-based compounds emit in the blue region? impact of the conjugation length and the ground-state aggregation. *Chem. Mater.* 2017, **29**, 1695–1707.
- 34 J. Zhou, P. Chen, X. Wang, Y. Wang, Y. Wang, F. Li, M. Yang, Y. Huang, J. Yu and Z. Lu, Charge-transfer-featured materials—promising hosts for fabrication of efficient OLEDs through triplet harvesting via triplet fusion, *Chem. Commun.*, 2014, **50**, 7586–7589.
- 35 M.A. Baldo, C. Adachi and S. R. Forrest, Transient analysis of organic electrophosphorescence. II. Transient analysis of triplet-triplet annihilation, *Phys. Rev. B*, 2000, **62**, 10967–10977.
- 36 T. Zhang, B. Chu, W. Li, Z. Su, Q. M. Peng, B. Zhao, Y. Luo, F. Jin, X. Yan, Y. Gao, H. Wu, F. Zhang, D. Fan and J. Wang, Efficient Triplet Application in Exciplex Delayed-Fluorescence OLEDs Using a Reverse Intersystem Crossing Mechanism Based on a  $\Delta E$  S–T of around Zero, *ACS Appl. Mater. Interfaces*, 2014, **6**, 11907–11914.
- 37 K. Goushi, K. Yoshida, K. Sato and C. Adachi, Organic light-emitting diodes employing efficient reverse intersystem crossing for triplet-to-singlet state conversion, *Nat. Photonics*, 2012, **6**, 253–258.
- 38 A. Y. Tomoaki Kozaki, Shota Koga, Naohiro Toda, Hiroki Noguchi, Effects of short wavelength control in polychromatic light sources on nocturnal melatonin secretion, *Neurosci. Lett.*, 2008, **439**, 256–259.